Journal of Solid State Chemistry **163,** 466–471 (2002)
doi:10.1006/jssc.2001.9429, available online at http://www.idealibrary.com on IDEAL®

Effect of the *A* Cation Size on the Structural, Magnetic, and Electrical Properties of Perovskites $(La_{1-x}Nd_x)_{0.7}Sr_{0.3}MnO_3$

K. Cherif,* J. Dhahri,*,[1] E. Dhahri,† M. Oumezzine, and H. Vincent‡

*Laboratoire de Physico-Chimie des Matériaux, Faculté des Sciences de Monastir, 5019 Monastir, Tunisia; †Laboratoire de Physique des Matériaux, Faculté des Sciences de Sfax, B.P. 763, Sfax, Tunisia; and ‡Laboratoire des matériaux et de Génie Physique, ENSPG, B.P. 46, 38402 Saint Martin d'Héres, Cedex, France

Received May 1, 2001; in revised form October 8, 2001; accepted October 15, 2001

An intense effort has recently been devoted to studying the interplay between structure, magnetism, and transport in manganese perovskite $Ln_{1-x}A_xMnO_3$ (Ln = La, Pr, Nd, Sm; A = Ca, Ba, Sr). As a function of temperature, applied magnetic field, doping, A-site ionic radius $\langle r_A \rangle$, and A-site size disorder, this system displays a rich phase diagram for both magnetotransport and structural properties. We have investigated the structural, magnetic, and transport properties of $(La_{1-x}Nd_x)_{0.7}Sr_{0.3}MnO_3$. The crystal structure was examined by X-ray powder diffraction which indicated that all the samples were single phase and revealed a transition from rhombohedral to orthorhombic structure with increasing x. The magnetization and resistivity investigation shows that for all values of x, $(La_{1-x}Nd_x)_{0.7}Sr_{0.3}MnO_3$ are ferromagnetic–metallic at low temperatures and paramagnetic–semiconductor above the Curie temperature T_c. © 2002 Elsevier Science (USA)

1. INTRODUCTION

The perovskite (Ln–A) MnO_3 (Ln = La, Pr, Nd_{min}; A = Pb, Ca, Cd, Ba, or Sr) is a fascinating magnetic system with diverse magnetically ordered structures as one varies the concentrations of dopant A (1–3). This results in a Mn^{3+}/Mn^{4+} mixed-valence state creating mobile charge carriers and canting of Mn spins (4). It is believed that the electrical properties are controlled by the motion of an e_g electron from a Mn^{3+} ($t_{2g}^3\ e_g^1$: $S = 2$) to a Mn^{4+} ($t_{2g}^3\ e_g^0$: $S = \frac{3}{2}$) via the intervening oxygen. The magnetic coupling between Mn^{3+} and Mn^{4+} is also correlated with the motion of the e_g electron between the two partially filled d shells with strong on-site Hund coupling. The electrical and magnetic properties have been understood within the framework of the double exchange (DE) model (5–8). The motion of the e_g electron can be strongly influenced by the average ionic radius of the A site $\langle r_A \rangle$ which exhibits a close relationship between the bending of the Mn–O–Mn bond angle and the narrowing of the electronic band width (9, 10). Intense interest in this system was revived after the discovery of colossal magnetoresistance (CMR) in the metallic phase of the system (11–13). It is remarkable that the magnetoresistance can be as large as 100-fold in polycrystalline $La_{0.60}Y_{0.07}Ca_{0.33}MnO_x$ (14) and 1000- to 10,000-fold in $La_{0.67}Ca_{0.33}MnO_{3+\delta}$ (15) and $Nd_{0.7}Sr_{0.3}MnO_{3-\delta}$ (13) epitaxial thin films.

The aim of this work is to study the effect of the substitution of nonmagnetic ion La^{3+} by the magnetic ion Nd^{3+} on the structural, magnetic, and electrical properties in $La_{0.7}Sr_{0.3}MnO_3$, which has a high ferromagnetic Curie temperature $T_C = 369$ K (16).

2. SAMPLE PREPARATION

The different manganites $(La_{1-x}Nd_x)_{0.7}Sr_{0.3}MnO_3$ were prepared as sintered ceramics by mixing La_2O_3, Nd_2O_3, $SrCO_3$, and MnO_2 in stoichiometric proportions. The mixtures were first heated in air at 1173 K for 3 days to achieve decarbonation. After grinding, they were heated again at 1473 K for 24 h and reground again to ensure homogenization. The powders were then pressed in the form of bars under 4 tons/cm^2 and sintered at 1673 K for 2 days in air with several periods of grinding and repelleting. Phase purity, structure, and lattice parameters were determined by powder X-ray diffraction with a Siemens D5000 using Cu$K\alpha$ radiation at room temperature. Lattice constants were obtained by least-squares calculations. In this series of samples, the average ionic radius of the A site $\langle r_A \rangle$ is systematically decreased due to the substitution of La (ionic radius of ~ 1.22 Å) by the smaller Nd (ionic radius of ~ 1.15 Å), while the carrier concentration remain fixed.

The magnetization M of the samples as a function of temperature at 500 Oe was measured using a home-built Faraday-type balance.

[1]To whom correspondece should be addressed. E-mail: jemai.dhahri@fsm.rnu.tn. Fax: + 2163500274.

0022-4596/02 $35.00

Resistivity measurements in the absence of an applied field were performed using a standard four-probe method for all samples. The sample was cut into a square shape, with a typical dimension of $(1 \times 5 \times 5)$ mm^3.

3. RESULTS AND DISCUSSION

3.1. X-Ray Analysis

X-ray diffraction patterns of several representative samples are shown in Fig. 1 ($x = 0.1, 0.2, 0.5$, and 1). No traces of secondary phases were detectable, within the sensitivity limits of the experiment (a few percent). The diffraction peaks are sharp and can be indexed on either a rhombohedral cell for 1.2203 Å $\leq \langle r_A \rangle \leq$ 1.2350 Å on an orthorhombic cell for $\langle r_A \rangle <$ 1.2203 Å.

The structural transitions in the $(La_{1-x}Nd_x)_{0.7}Sr_{0.3}MnO_3$ series are governed by the size of the rare-earth ions La^{3+} and Nd^{3+}. The smaller Nd^{3+} ion induces a transformation to orthorhombic symmetry at high values of x ($x \geq 0.5$). The exact concentrations at which the transformations to orthorhombic symmetry for the Nd series occur are difficult to determine from powder X-ray data. A similar phase transition from rhombohedral to orthorhombic structure was observed in the $La_{0.7-x}Pr_xSr_{0.3}MnO_3$ compounds (17) whereas $La_{0.7-x}Pr_xCa_{0.3}MnO_3$ and $La_{0.7-x}Y_xCa_{0.3}MnO_3$ compositions are single phase with an orthorhombic (*Pbnm*) perovskite structure (9, 18).

The variation of lattice parameters and the unit cell volume as a function of $\langle r_A \rangle$ is shown in Figs. 2 and 3, respectively.

It can be seen that the unit cell volume decreases when $\langle r_A \rangle$ decreases. This result can be explained by the change of the Mn–O–Mn bond angle. Indeed, in the perovskite $LaMnO_3$, the manganase ions are surrounded by regular octahedra of oxygens (MnO_6) which are linked together by their corners to form a three-dimensional framework, while the La ions occupy the A site between these octahedra. For a perfect size match (tolerance factor $t = 1$ (19)), the Mn–O–Mn bond angle θ would be 180°. With a decrease of the average ionic radius, by substituting La^{3+} ions by smaller Nd^{3+} ions, the octahedra tilt and rotate to reduce the excess space around the A site, leading to ($\theta = 180° - \phi$, where ϕ increases with the decrease of $\langle r_A \rangle$ (20). Therefore, the Mn–Mn distances decrease and the unit cell volume decreases with decreasing $\langle r_A \rangle$. The relationship between $\langle r_A \rangle$ and Mn–O–Mn bond angle θ has been confirmed for our samples by powder X-ray diffraction at room tempearture using the standard Rietveld profile refinement (Table 1).

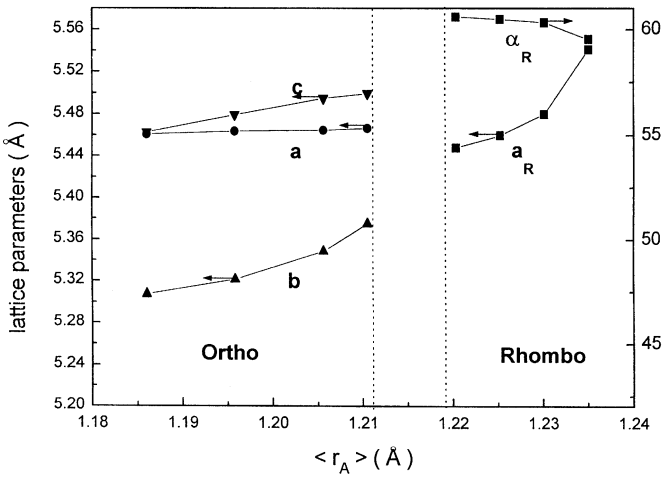

FIG. 2. Variation of lattice parameters with $\langle r_A \rangle$ for $(La_{1-x}Nd_x)_{0.7}Sr_{0.3}MnO_3$.

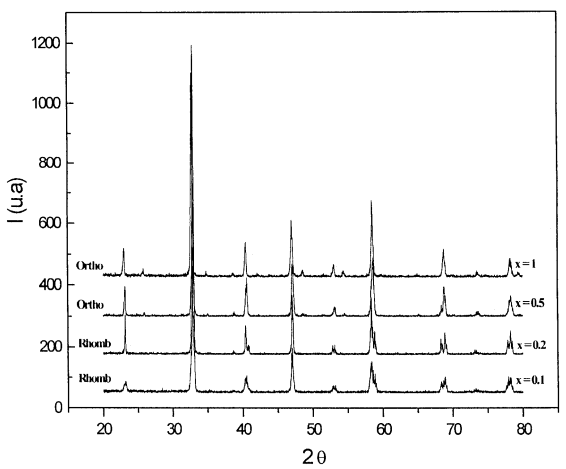

FIG. 1. X-ray diffraction patterns at room temperature of $(La_{1-x}Nd_x)_{0.7}Sr_{0.3}MnO_3$ for $x = 0.1, 0.2, 0.5$, and 1.

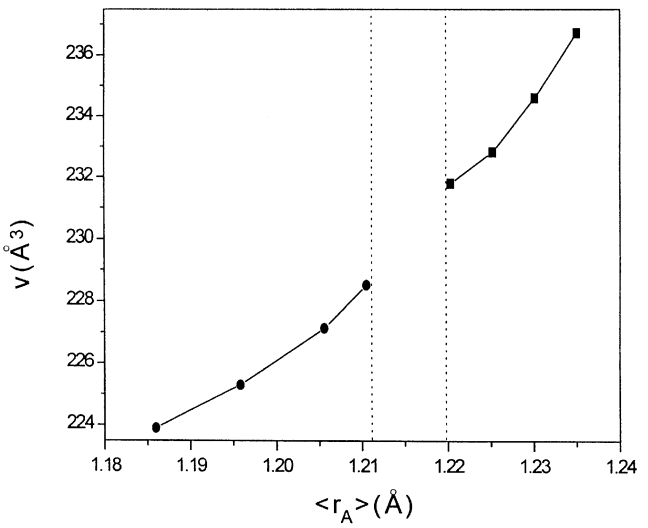

FIG. 3. Variation of unit cell volume with $\langle r_A \rangle$ for $(La_{1-x}Nd_x)_{0.7}Sr_{0.3}MnO_3$.

TABLE 1
Selected Structural Parameters at Room Temperature[a]

	X						
	0	0.1	0.2	0.3	0.5	0.8	1
Structure	Rhombo	Rhombo	Rhombo	Rhombo	Ortho	Ortho	Ortho
dMnMn (Å)	3.887(1)	3.884(1)	3.881(1)	3.877(2)	3.869(2)	3.859(2)	3.856(2)
dMn–OI (Å)	1.957(2)	1.957(1)	1.958(2)	1.959(2)	1.965(2)	1.963(2)	1.961(1)
dMn–OII (Å)	—	—	—	—	1.979(1)	1.973(1)	1.969(2)
dMn–OII (Å)					1.952(2)	1.957(2)	1.962(2)
θMn–OI–Mn	166.3(1)	165.2(1)	164.3(1)	163.1(1)	161.0(1)	158.5(1)	157.0(1)
θMn–OII–Mn	—	—	—	—	162.3(2)	160.4(2)	159.0(1)
$\langle r_A \rangle$	1.235	1.230	1.225	1.220	1.210	1.195	1.186

[a]In the orthorhombic structure, there are two distinct oxygen sites: the out-plane o_I and the planar o_{II}.

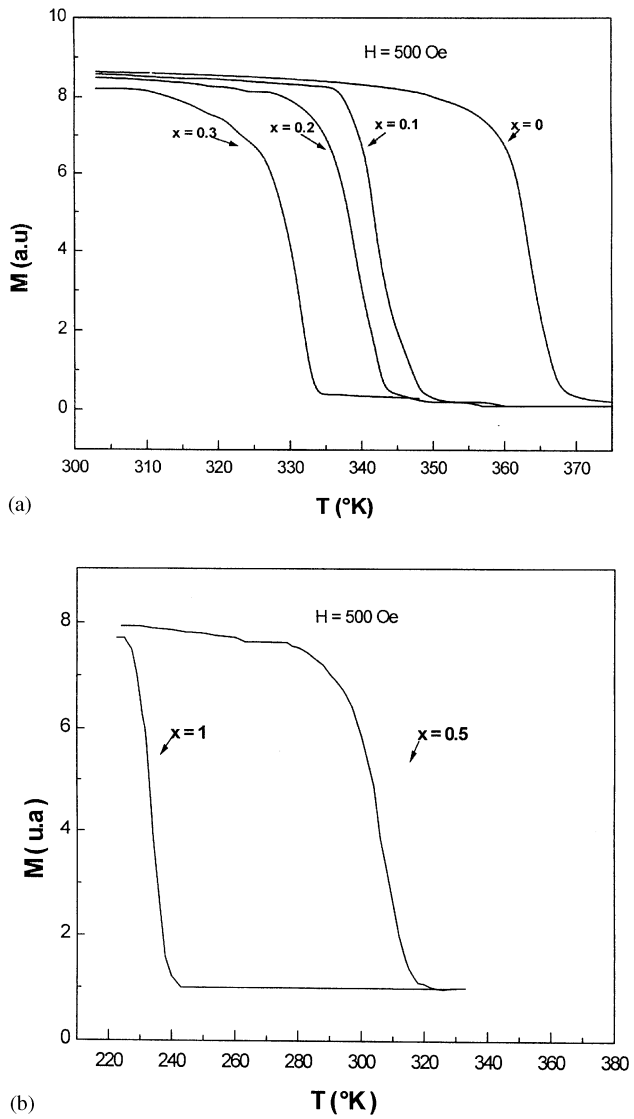

FIG. 4. Magnetization (in arbitrary units) as a function of temperature at 500 Oe for $x = 0$, 0.1, 0.2, 0.3, 0.5, and 1 in $(La_{1-x}Nd_x)_{0.7}Sr_{0.3}MnO_3$.

In comparison to $La_{0.7}Sr_{0.3}MnO_3$ and $Nd_{0.7}Sr_{0.3}MnO_3$, X-ray structure refinement revealed that the lattice distortion in $(La_{1-x}Nd_x)_{0.7}Sr_{0.3}MnO_3$ is larger than that in $La_{0.7}Sr_{0.3}MnO_3$ but smaller than that in $Nd_{0.7}Sr_{0.3}MnO_3$; e.g., the average bond angles varied from 166.3° in $La_{0.7}Sr_{0.3}MnO_3$ to 157.0° in $Nd_{0.7}Sr_{0.3}MnO_3$.

3.2. Magnetic Characterization

The investigation of the magnetic properties measured in a magnetic field of 500 Oe shows that all samples exhibit a single magnetic transition and behave in a ferromagnetic manner at low temperatures ($T \leq T_C$) and in a paramagnetic manner above the Curie temperature $T_C(T \geq T_C)$ (Fig. 4).

The Curie temperature T_C decreases when x increases in the $(La_{1-x}Nd_x)_{0.7}Sr_{0.3}MnO_3$ series (Fig. 5). The T_C variation has been interpreted by the increase of the Mn–O–Mn bond angle as $\langle r_A \rangle$ increases. In fact, the substitution of La by Nd should not change the Mn^{3+}/Mn^{4+} ratio but the difference in ionic size affects the Mn–O–Mn bond angle, which causes a narrowing of the bandwidth (e_g), resulting in a gradual enhancement of the effective band gap. As a consequence, the transfer interaction of e_g electrons should be reduced. Our previous magnetic measurements for $(La_{1-x}Nd_x)_{0.7}Sr_{0.3}MnO_3$ series show that the variation of the Curie temperature T_c is similar to that observed in $La_{0.7-x}A_xCa_{0.3}MnO_3$ (A = Y, Pr) (9, 18), $La_{0.7-x}Pr_xSr_{0.3}MnO_3$ (17), $A_{0.5-x}A'_xSr_{0.5}MnO_3$ (A, A' = Sm, La, Pr, Y, and Gd) (21), $La_{0.7}Sr_{0.3-x}Ca_xMnO_3$ (22), and $La_{0.6}Sr_{0.4-x}Ca_xMnO_3$ (23) but different from that observed in $La_{0.6}Ba_{0.4-x}Sr_xMnO_3$ (23) where T_c decreases when the average size $\langle r_A \rangle$ increases. The difference in the T_c variation in the Ba–Sr series can be interpreted by the great discrepancy between La^{3+} and Ba^{2+} sizes. The variation of the Curie temperature T_c as a function of the average ionic radius $\langle r_A \rangle$ for some examples is represented in Fig. 5.

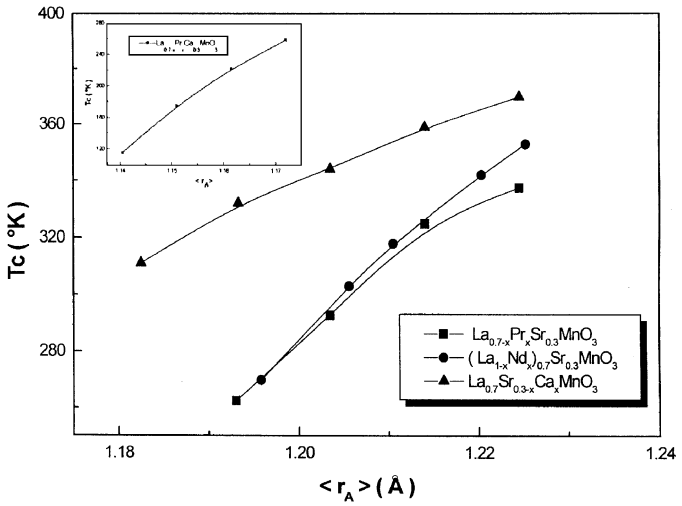

FIG. 5. Dependence of T_C on $\langle r_A \rangle$ for $(La_{1-x}Nd_x)_{0.7}Sr_{0.3}MnO_3$, $La_{0.7-x}Pr_xSr_{0.3}MnO_3$, and $La_{0.7}Sr_{0.3-x}Ca_xMnO_3$ samples. Inset: Dependence of T_C on $\langle r_A \rangle$ for $La_{0.7-x}Pr_xCa_{0.3}MnO_3$ samples.

Recent studies of $La_{0.7}A_{0.3}MnO_3$ (24) and $Ln_{0.5}A_{0.5}MnO_3$ (25) show that a second factor, the variance σ^2 of the A cation radii distribution, governs the transition temperature T_C. The mismatch effect represented by the variance σ^2 is defined by the relation

$$\sigma^2 = \sum y_i r_i^2 - \langle r_A \rangle^2,$$

where r_i is the radius of the various A site cations and y_i are their fractional occupancies ($\sum_i y_i = 1$). In the $(La_{1-x}Nd_x)_{0.7}Sr_{0.3}MnO_3$, T_C increases and σ^2 decreases when $\langle r_A \rangle$ increases. Figure 6 shows the variation of T_c with the cation size variance σ^2 for some examples of manganite perovskites with fixed ratio Mn^{3+}/Mn^{4+} and with constant $\langle r_A \rangle = 1.205$ Å. We have noted that the variation of T_c values measured for the samples having the same $\langle r_A \rangle$ is proportional to their σ^2.

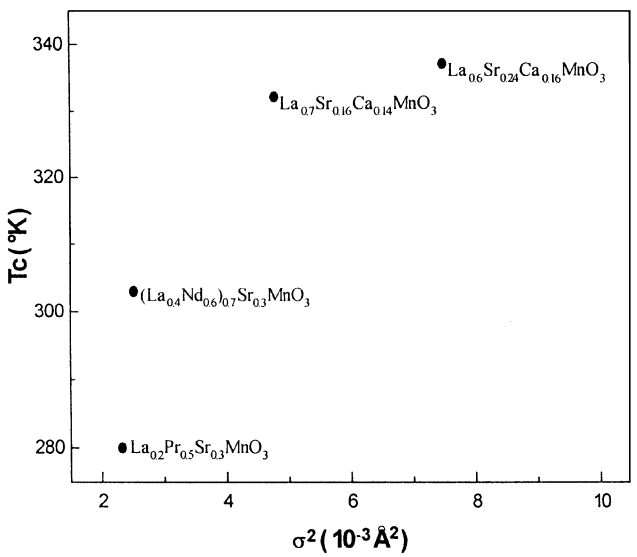

FIG. 6. Variation of T_c with A cation size variance σ^2 ($\langle r_A \rangle = 1.205$ Å).

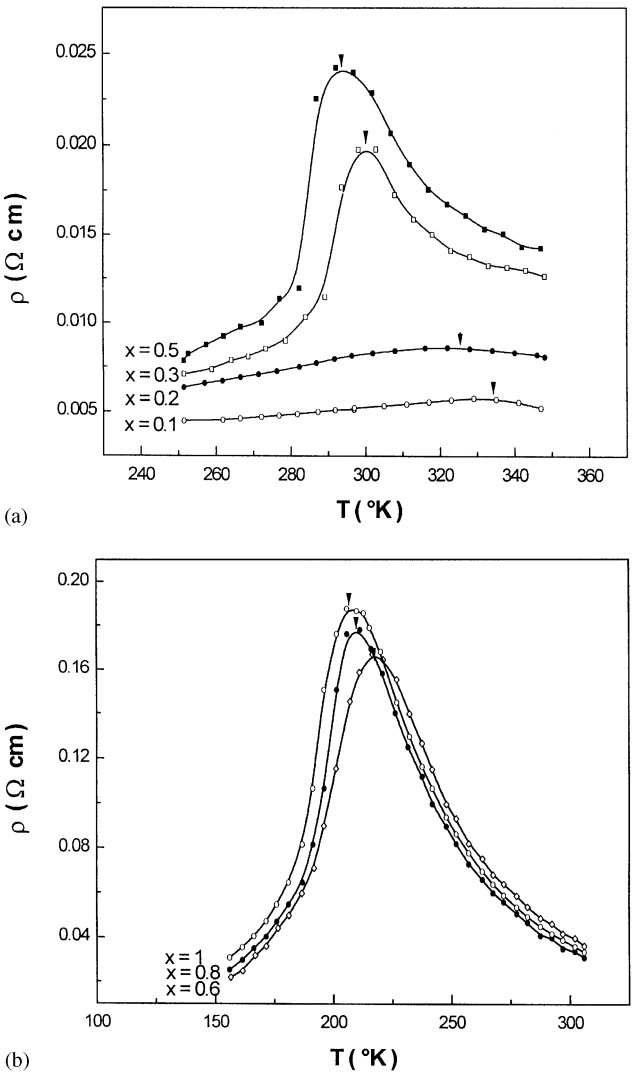

FIG. 7. Temperature dependence of the resistivity (a) $x = 0$, 0.1, 0.2, 0.3, and 0.5 and (b) $x = 0.6$, 0.8, and 1 for $(La_{1-x}Nd_x)_{0.7}Sr_{0.3}MnO_3$. (The temperature peak T_p is indicated by arrows.)

3.3. *Electric Characterization*

Using the sign of the temperature coefficient of resistivity as a criterion $(d\rho/dT) < 0$ for a semiconductor-like system and $(d\rho/dT) > 0$ for a metallic system, we found that all the compounds are ferromagnetic-metallic at low temperature ($T < T_p$) and paramagnetic semiconductor above T_p.

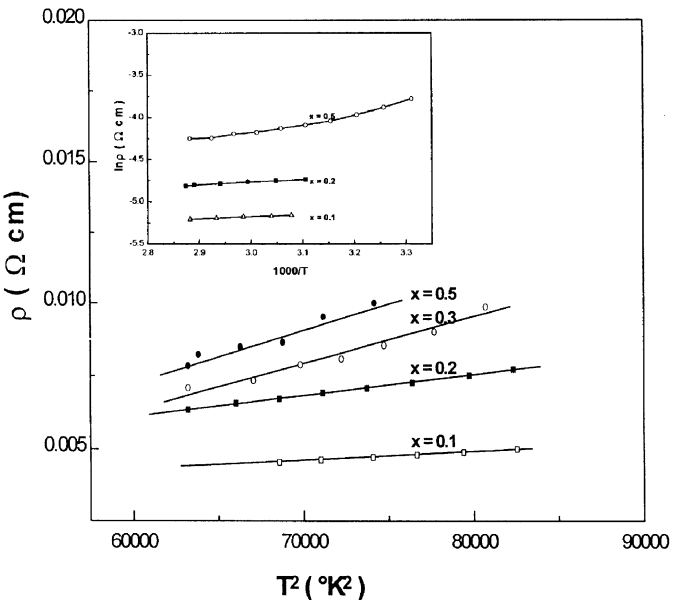

FIG. 8. Temperature dependence of resistivity in the low-temperature ferromagnetic regime ($T < 292$ K) for $(La_{1-x}Nd_x)_{0.7}Sr_{0.3}MnO_3$. The T^2 dependence of resistivity $(\rho T) = \rho(0) + AT^2$ was observed. Inset: $\log(\rho)$ as a function of $1/T$ for $x = 0.1$, 0.2, and 0.5.

The resistivity temperature peak T_p (indicated by arrows in Fig. 6) decreases and the resistivity peak ρ_{T_p} increases with increasing x (decreasing $\langle r_A \rangle$).This phenomenon can be interpreted as a gradual bending of the Mn–O–Mn bond angle with decreasing $\langle r_A \rangle$, which causes the narrowing of the bandwidth and results in a reduced mobility of the e_g electrons.

In the low-temperature ferromagnetic regime, the tempearture dependence of the resistivity for all the samples is described by quadratic function of temperature (Fig. 7):

$$\rho(T) = \rho(0) + AT^2 (T \leq 292 \text{ K}).$$

In typical ferromagnetic metals this term amounts to $0.299 \times 10^{-7}\,\Omega\,\text{cm}\,\text{K}^{-2} \leq A \leq 1.87\ \ 10^{-7}\ \ \Omega\,\text{cm}\,\text{K}^{-2}$. This result suggests the important role of the electron–electron scaterring process (16, 17).

At high temperature, in the paramagnetic phase ($T > T_p$), the conduction is thermally activated, indicating a conduction by magnetic polarons.

For samples with $x = 0.1$, 0.2, and 0.5, above T_p the resistivity obeys the standard relation

$$\rho = \rho_0 \exp(E_{hop}/KT),$$

where ρ_0 is a preexponential coefficient and E_{hop} is the hopping energy.

From the linear part of the curves $\log(\rho) - 1/T$, we deduce that the values of E_{hop} are 22.7 meV, 28 meV, and 90 meV, respectively. The difference in the E_{hop} values may be related to the existence of the transition from the rhombohedral ($x < 0.5$) to the orthorhombic structure.

4. CONCLUSION

The study of $(La_{1-x}Nd_x)_{0.7}Sr_{0.3}MnO_3$ shows that there is a structure transition due to the substitution of La^{3+} by Nd^{3+}. For $x \leq 0.3$ the structure is rhombohedral but for $x \geq 0.5$ the structure become orthorhombic. The investigation of magnetization measurements shows that all samples behave in a ferromagnetic manner at low temperature ($T \leq T_C$) and in a paramagnetic manner above the Curie temperature T_C. The T_C temperature decreases when x increases. The electrical studies of this manganese perovskite with a fixed carrier concentration, i.e., the ratio of Mn^{3+}/Mn^{4+} fixed, shows that the value of the resistance increases when the level of Nd increases. The resistivity dependence on temperature shows a transition from metal to semiconductor phase. The structural, magnetic, and electrical properties are correlated with the change of Mn–O–Mn bond angle.

REFERENCES

1. E. O. Wollan and W. C. Koehler, *Phys. Rev.* **100,** 545 (1955).
2. G. H. Jonker, *Physica* **22,** 707 (1956).
3. Y. Tokura, A. Urushibara, Y. Moritoma, and T. Arima, *J. Phys. Soc. Jpn.* **63,** 3991 (1994).
4. Z. Jirak, F. Damay. M. Hervieu, and C. Martin, *Phys. Rev. B* **61,** 1181 (2000).
5. C. Zener, *Phys. Rev.* **82,** 403 (1951).
6. P. G. de Gennes, *Phys. Rev.* **118,** 141 (1960).
7. P. W. Anderson and H. Hasegawa, *Phys. Rev.* **100,** 675 (1955).
8. K. Kubo and N. Ohata, *J. Phys. Soc. Jpn.* **33,** 21 (1972).
9. H. Y. Hwang, S. W. Cheong, and P. G. Radalli, *Phys. Rev. Lett.* **75,** 914 (1995).
10. Z. B. Guo, N. Zhang, W. P. Ding, and W. Yang, *Solid State Commun.* **100,** 769 (1996).
11. S. Stadler and Y. U. Idzerda, *Appl. Phys. Lett.* **75,** 3384 (1999).
12. J. Z. Sun and D. W. Abraham, *Appl. Phys. Lett.* **74,** 3017 (1999).
13. G. C. Xing, Q. Li, H. L. Ju, S. N. Mao, and L. Senapati, *Appl. Phys. Lett.* **66,** 1427 (1995).
14. S. Jin, H. M. O'Bryan, T. H. Tiefel, and M. McCormack, *Appl. Phys. Lett.* **66,** 382 (1995).
15. S. Jin, T. H. Tiefel, M. McCormack, R. A. Fastnacht, R. Ramesh, and L. H. Chen, *Science.* **264,** 413 (1994).
16. A. Urushibara, Y. Moritomo, T. Arima, A. Asamitsu, G. Kido, and Y. Tokura, *Phys. Rev. B* **51**(20), 14103–14109 (1995).
17. Z. Guo, J. Zhang, N. Zhang, W. Ding, He Huang, and Y. Du, *Appl. Phys. Lett.* **70**(14), 1897–1899 (1997).
18. J. Fontcuberta, B. Martinez, A. Seffar, S. Pinol, J. L. Gareia-Munoz, and X. Obradors, *Phys. Rev. Lett.* **76**(7), 1122–1125 (1996).
19. V. Golovanov, L. Mihaly, and A. R. Moudenbaugh, *Phys. Rev. B* **53**(13), 8207–8210, (1996).
20. J. R. Sun, G. H. Rao, and J. K. Liang, *Appl. Phy. Lett.* **70**(14), 1900–1902 (1997).
21. F. Damay, A. Maignon, C. Martin, and B. Raveau, *J. Appl. Phys.* **81**(3), 1372–1377 (1997).

22. N. Abdelmoula, J. Dhahri, K. Guidara, E. Dhahri, and J. C. Joubert, *Phase Transit*. **70,** 197–210 (1999).
23. N. Abdelmoula, J. Dhahri, K. Guidara, E. Dhahri, and J. C. Joubert, *Phase Transit*. **70,** 211–222 (1999).
24. L. M. Rodriguez-Martinez and J. P. Attfield, *Phy. Rev. B*, **54,** 15622–15625 (1996).
25. F. Damy, C. Martin, A. Magnan, and B. Raveau, *J. Appl. Phys.* **82**(12), 6181–6185 (1997).